Analysis of proton-induced fragment production cross sections by the quantum molecular dynamics plus statistical decay model

Satoshi Chiba,[1,2] Osamu Iwamoto,[2] Tokio Fukahori,[1,2] Koji Niita,[1,3]
Toshiki Maruyama,[1] Tomoyuki Maruyama,[1] and Akira Iwamoto[1]
[1]*Advanced Science Research Center, Japan Atomic Energy Research Institute, Tokai-mura, Naka-gun, Ibaraki-ken 319-11, Japan*
[2]*Nuclear Data Center, Japan Atomic Energy Research Institute, Tokai-mura, Naka-gun, Ibaraki-ken 319-11, Japan*
[3]*Research Organization for Information Science and Technology Tokai-mura, Naka-gun, Ibaraki-ken 319-11, Japan*
(Received 7 February 1996)

The production cross sections of various fragments from proton-induced reactions on ^{56}Fe and ^{27}Al have been analyzed by the quantum molecular dynamics (QMD) plus statistical decay model (SDM). It was found that the mass and charge distributions calculated with and without the statistical decay have very different shapes. These results also depend strongly on the impact parameter, showing an importance of the dynamical treatment as realized by the QMD approach. The calculated results were compared with experimental data in the energy region from 50 MeV to 5 GeV. The QMD+SDM calculation could reproduce the production cross sections of the light clusters and intermediate-mass to heavy fragments in a good accuracy. The production cross section of ^{7}Be was, however, underpredicted by approximately 2 orders of magnitude, showing the necessity of another reaction mechanism not taken into account in the present model. [S0556-2813(96)02807-5]

PACS number(s): 24.10.−i, 02.70.Ns, 25.40.−h

I. INTRODUCTION

Recently we have developed a framework of the quantum molecular dynamics (QMD) plus statistical decay model (SDM) that takes account of the relativistic kinematics and relativistic correction for interaction term, Lorentz boost of the initial and final states, realistic momentum distribution in the ground state, and comprehensive nucleon-nucleon (NN) collision term [1]. It was shown [1] that this framework could reproduce the measured double-differential (p,xn), (p,xp') and $(p,x\pi)$ reactions from 100 MeV to 3 GeV in a systematic way. In the subsequent papers [2,3], we have given detailed analyses of the preequilibrium (p,xp') and (p,xn) reactions in terms of the QMD in the energy region of 100–200 MeV. It was demonstrated that the Fermi motion including the high-momentum component, surface refraction, multistep effect and the multiple preequilibrium emission were the key issues in understanding the angular distributions of neutrons and protons emitted during the preequilibrium process. In these analyses a single set of parameters was selected, and no adjustment was attempted.

The success obtained in the previous studies has shown the ability of the QMD+SDM approach for the study of the nucleon-induced nuclear reactions. However, the previous analyses have been concentrated on the inclusive particle spectra, and a fine selection of the final reaction products was not performed. It is therefore the purpose of this work to carry out an analysis of proton-induced reactions for the production of specific final states, i.e., fragments, with the same formulae and the same set of parameters as the previous works [1–3] to investigate further the validity of the QMD +SDM approach. Such fragmentation phenomena themselves have been a matter of long and intensive studies to extract the basic reaction mechanisms of nucleon-induced reactions [4–9], e.g., multifragmentation, liquid-gas phase transition, sideward peaking of fragment angular distribution, properties of nuclei at high temperature, etc. Reliable estimations of fragment production are also important in many application fields [10–16].

In this work, the fragment production cross sections from $p+^{56}$Fe and $p+^{27}$Al reactions were calculated. These targets were selected because (1) they are monoisotopic or nearly monoisotopic in the natural elements, therefore the data are abundant, (2) they are popular elements among the structural

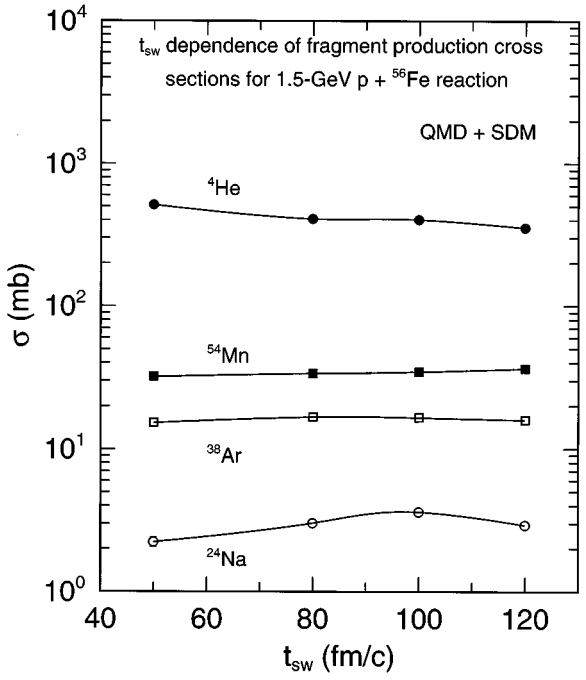

FIG. 1. Dependence of the production cross sections of ^{4}He, ^{24}Na, ^{38}Ar, and ^{54}Mn on the switching time, t_{sw}, from the QMD to SDM calculation for 1.5-GeV $p+^{56}$Fe reaction.

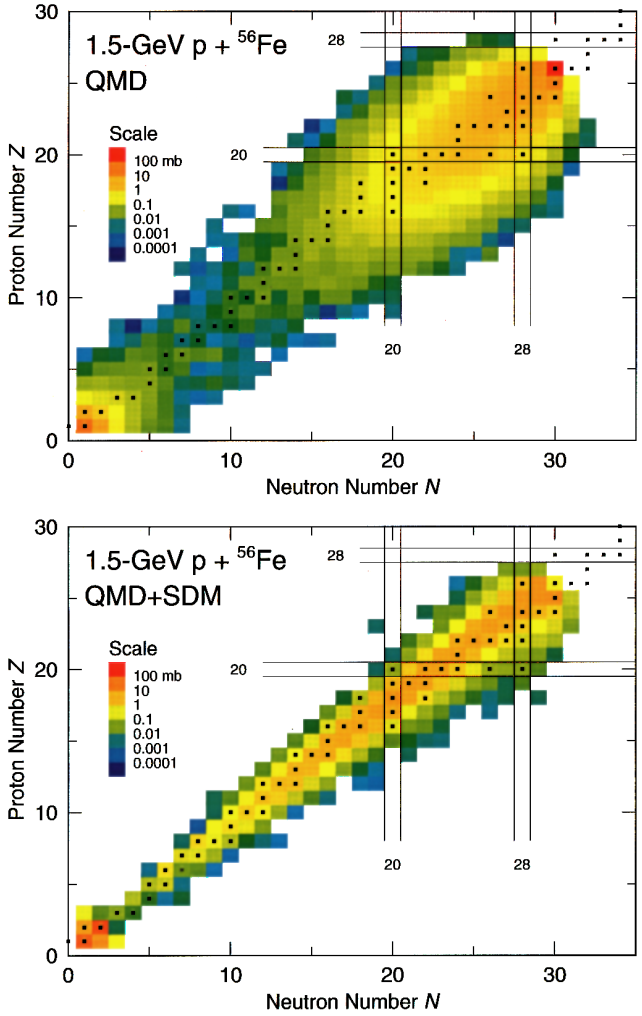

FIG. 2. Distribution of various fragments in the N-Z plane from the QMD alone (top) and QMD+SDM (bottom) calculations for 1.5-GeV proton + ^{56}Fe reaction. The small squares indicate positions of stable isotopes, while vertical and horizontal lines at $N,Z=20$ and 28 denote the magic numbers.

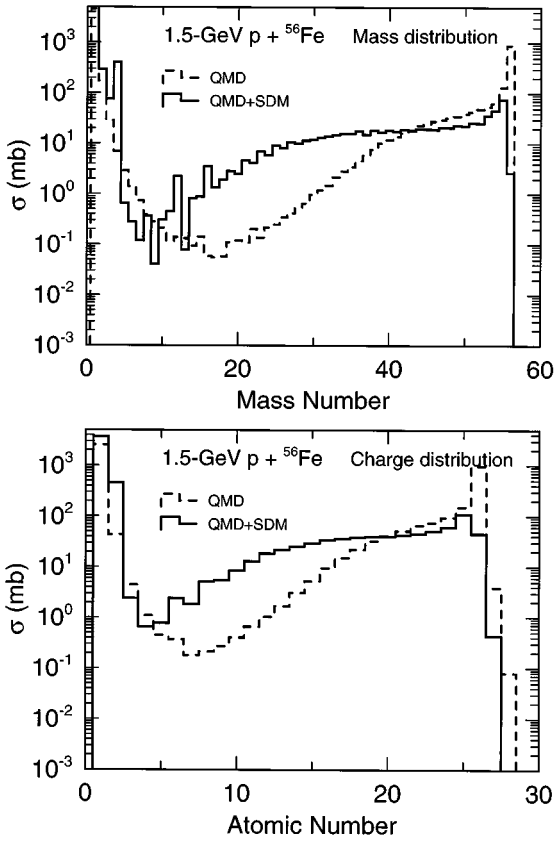

FIG. 3. Calculated mass (top) and charge (bottom) distributions of fragments for 1.5-GeV $p+^{56}$Fe reaction. The broken histograms show the results for QMD calculation only, while the solid ones corresponding to QMD+SDM results.

materials with high importance from the practical point of view, and (3) effects of the fission and multifragmentation become significant for heavier elements, where an analysis is too complicated. Moreover, the computation time, proportional to the square of the mass number, is kept manageable for these target materials. Special emphasis was placed for the proton energy of 1.5 GeV because this energy attracts special attention as a possible candidate energy of application of a high-intensity proton accelerator for researches on transmutation of radioactive wastes and basic sciences [17]. The maximum energy was chosen to be 5 GeV: above this energy many nucleon-nucleon inelastic channles, which are not considered in our model, are open.

In the next section, a brief explanation of the QMD plus SDM approach is given. The comparison of the calculation with the experimental data and discussions on the reaction mechanisms are given in Sec. III. A summary of this work is given in Sec. IV.

II. ESSENCE OF THE QMD PLUS SDM MODEL

The details of the QMD and SDM calculations are given in Ref. [1], so only the basic principles of them will be repeated here. In the QMD calculation, each nucleon is expressed with a Gaussian wave packet in both the coordinate and momentum spaces in the following way:

$$f_i(\mathbf{r},\mathbf{p})=8\ \exp\left[-\frac{(\mathbf{r}-\mathbf{R}_i)^2}{4L}-\frac{2L(\mathbf{p}-\mathbf{P}_i)^2}{\hbar^2}\right], \qquad (1)$$

where L is a parameter which represents the spacial spread of a wave packet, $\mathbf{R}_i$ and $\mathbf{P}_i$ corresponding to the centers of a wave packet in the coordinate and momentum spaces, respectively. The total one-body phase-space distribution function is taken to be simply a sum of these single-particle wave packets. Initially, we distribute the $\mathbf{R}_i$ and $\mathbf{P}_i$ to produce a stable target ground state with realistic density and momentum distributions. The time evolution of $\mathbf{R}_i$ and $\mathbf{P}_i$ is determined based on the Newtonian equation and the NN collision term, latter satisfying the Pauli exclusion principle. A Skyrme-type interaction parametrized in Ref. [1] is used as the effective interaction. In addition, the symmetry and the Coulomb forces are included.

The QMD calculation is carried out up to a time scale 100 (fm/c), which is referred to as the switching time, t_{sw}. The position and momentum of each nucleon is then used to cal-

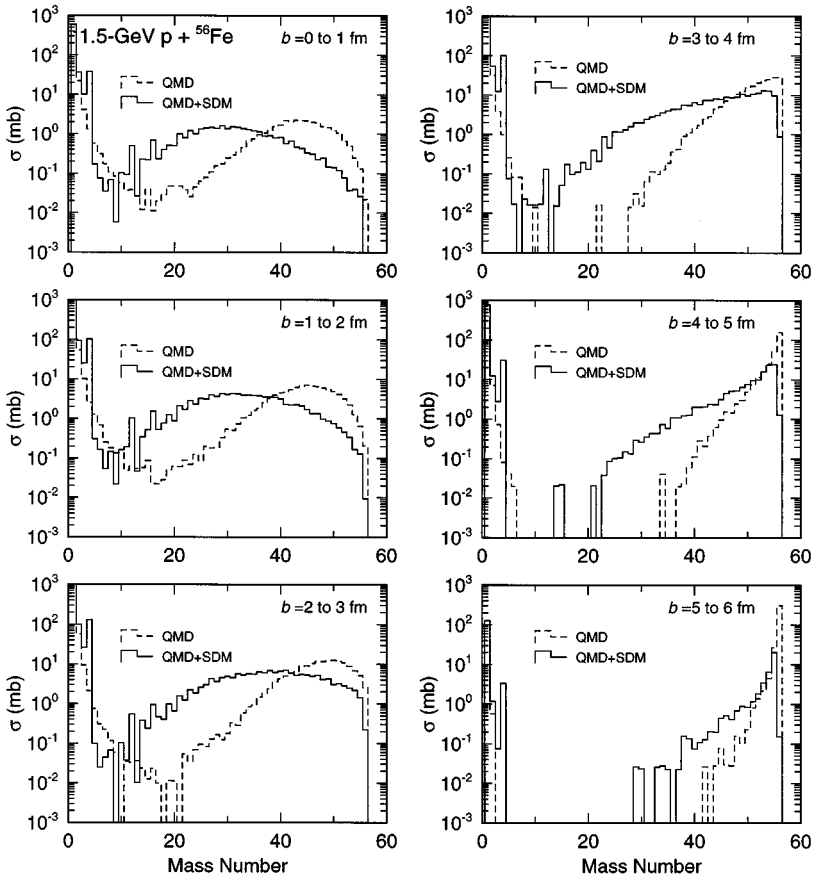

FIG. 4. Calculated mass distributions for 1.5-GeV $p+{}^{56}$Fe reaction with different impact parameters.

culate the distribution of mass and atomic numbers, kinetic energy and direction of motion of the remaining fragments (referred to as ''prefragments'') as well as those of the emitted nucleons and π mesons. In determining the mass and atomic numbers of the prefragments, the phase-space minimum-distance-chain method [18] is employed.

The prefragments thus identified are then Lorentz boosted into their rest frames to evaluate their excitation energies. When the prefragment is in the excited state, the statistical decay via n, p, d, t, ^{3}He, and α emissions is considered based on the Weisskopf-Ewing approximation, the emission probability of particle x being given as

$$P_x=(2J_x+1)m_x\epsilon\sigma_x(\epsilon)\rho(E)d\epsilon, \tag{2}$$

where J_x, m_x, and ϵ are the spin, mass, and kinetic energy of the emitted particle, while $\sigma_x(\epsilon)$ and $\rho(E)$ denote the inverse cross section and the level density of the residual nucleus at the excitation energy E, respectively. The level density has been assumed to be proportional to $\exp(2\sqrt{aE})$ with $a=A/8$ MeV^{-1}. The inverse cross section is taken to be of the form $\sigma_x(\epsilon)=(1-U_x/\epsilon)\pi R^2$ if $\epsilon>U_x$ and $\sigma_x(\epsilon)=0$ otherwise, where R denotes the absorption radius and U_x is the empirical Coulomb barrier for particle x [19].

The separation of the QMD and SDM calculations as performed in this approach can give the individual production cross sections of various residues before and after the statistical decay, the former being called as the prefragment, the latter as the fragment. This possibility gives information on the relation of the dynamical and statistical processes as a function of projectile energy and impact parameter. On the contrary, this hybrid approach introduces an ambiguity because the switching time $t_{\rm sw}$ is an arbitrary parameter. As described above, we have selected $t_{\rm sw}$ to be 100 (fm/c), because this value was enough to obtain stable neutron spectra from the (p,xn) reaction against a change of $t_{\rm sw}$ as shown in Ref. [1]. However, it does not necessarily mean that this value is also appropriate to obtain stable values for more exclusive observables as the fragment production cross sections. Therefore, we have carried out calculations by changing the value of $t_{\rm sw}$, and investigated how various fragment production cross sections would vary as a function of this parameter. The result is shown in Fig. 1 for the production of ^{4}He, ^{24}Na, ^{38}Ar, and ^{54}Mn for 1.5-GeV $p+{}^{56}$Fe reaction. This is a result of the QMD plus SDM calculation. This figure demonstrates that the cross section values given by the present approach are very robust against the change of the switching time $t_{\rm sw}$, therefore defines the cross sections in a unique way at around $t_{\rm sw}=100$(fm/c).

Calculations with event number of 50 000 for each combination of target and proton energy have been performed to get enough statistical accuracy. The computation time was approximately 24 h for the $p+{}^{56}$Fe reaction on HP9000/735 work station.

III. RESULTS AND DISCUSSION

Calculated cross sections for the production of various prefragments and fragments are shown for 1.5-GeV $p+{}^{56}$Fe reaction in Fig. 2. Here the upper figure shows the production cross sections calculated only by the QMD, while

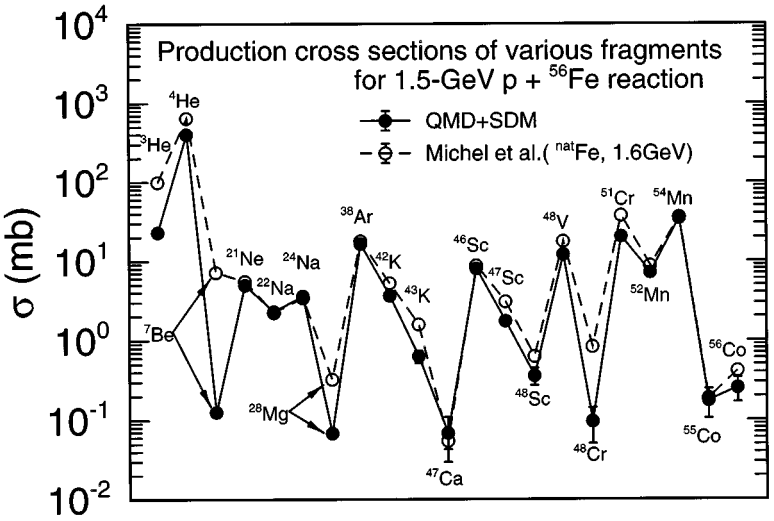

FIG. 5. Production cross sections of various fragments for 1.5-GeV proton + ^{56}Fe reaction. The solid circles connected by a solid line denote the result of QMD+SDM calculation, while the open circles connected by a broken line were obtained experimentally by Michel *et al.* measured at 1.6 GeV for ^{nat}Fe.

the lower one is obtained including the statistical decay. In this and the subsequent figures, the cross sections before and after the statistical decay process is denoted as the ''QMD'' and ''QMD+SDM,'' respectively. The small squares indicate the positions of stable nuclei, while the lines at $N,Z=20$ and 28 show the locations of major magic numbers. The upper part of Fig. 1 shows that the prefragments are produced primarily in mass $A = 1$–10 and $A_T/2 \leqslant A \leqslant A_T$ regions, with A_T as the target mass. In the cascade model approach [20,21], the light mass fragments ($A \leqslant 10$) are produced only as a result of the statistical decay or as a spallation residue, whereas the QMD describes the dynamical emission of such light mass fragments as shown in Fig. 2. This is a clear advantage of the QMD approach. The intermediate-mass-fragment (IMF) corresponding to mass 10 to $A_T/2$ are very rare (about an order of 10–100 μ b) in the QMD result alone. In the target region, the prefragments are distributed in a broad area of the N-Z plane. This distribution, then, is changed via the statistical decay to the bottom figure which is more localized along the stability line. The IMF region is primarily filled by the statistical decay of heavier prefragments, and the final isotopic distribution becomes significantly flattened in the direction of the stability line as a result of the statistical decay. At the same time, the yield of the light mass fragment becomes much larger, in particular of α particle. Figure 2 demonstrates clearly the importance of both the dynamical and statistical processes which are included in the QMD+SDM approach.

Figure 3 shows the total mass (top figure) and charge (bottom figure) distributions from the QMD and QMD +SDM calculations for the same projectile-target combination. This figure again confirms that the QMD calculation predicts dynamical production of the light ($A \leqslant \sim 10$) and target mass-charge regions. The statistical decay then makes the distributions much smoother and flatter. The IMF is produced primarily by the statistical decay.

In Fig. 4, the mass distributions obtained for 1.5-GeV $p+^{56}$Fe reaction with different impact parameter events are shown. In this figure the impact parameter (denoted as b) varies from 0 to 1 fm in the left-top figure, then the impact parameter range is increased in steps of 1 fm toward the right-bottom one. The total mass-yield distributions given in the upper part of Fig. 3 were obtained by integrating the contributions from the whole impact parameter range given in Fig. 4. Figure 4 indicates that the mass distribution changes significantly as a function of the impact parameter.

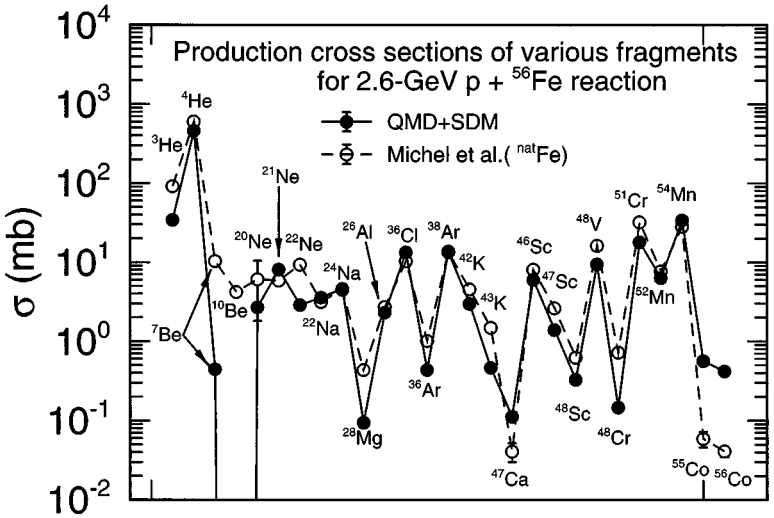

FIG. 6. Production cross sections of various fragments for 2.6-GeV proton + ^{56}Fe reaction. The solid circles connected by a solid line denote the result of QMD+SDM calculation, while the open circles connected by a broken line were obtained experimentally by Michel *et al.*

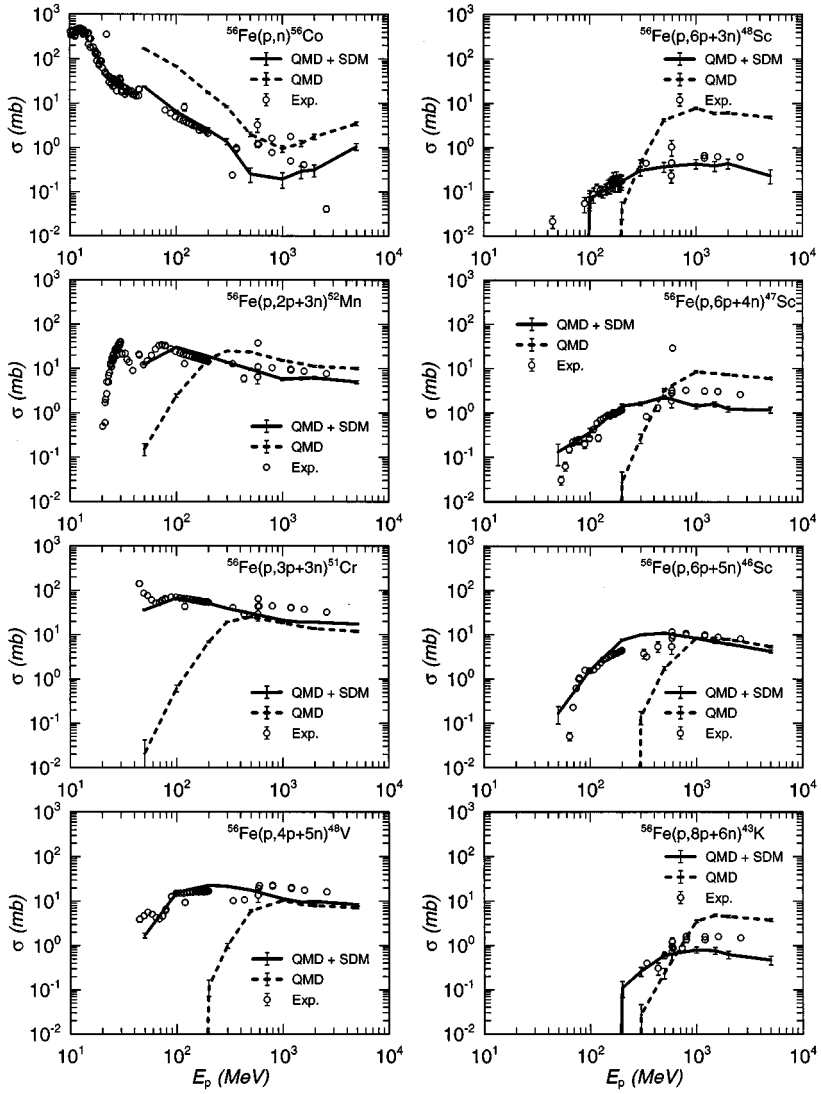

FIG. 7. Calculated and measured fragment production cross sections for the $p+{}^{56}$Fe reaction as a function of incident energy.

For the events having smaller impact parameters, the QMD distribution has a broad maximum centered around a mass of 45. Then this distribution becomes much broadened by the statistical decay, shifting the peak to around mass $\sim A_T/2$. As the impact parameter increases, the distribution is shifted toward higher masses; at the peripheral events ($b \geqslant 4$ fm) the QMD distribution has a sharp peak at the target mass. In this impact parameter region, the incident proton interacts with a nucleon by grazing the target near the surface. Therefore the chance that one of these two nucleons is emitted from the target without further collisions is very high due to a smaller nucleon density than in the central region. For such a reaction, which may be referred to as a ''one-step'' reaction, the cross section is determined by the magnitude of the basic nucleon-nucleon cross section. Furthermore, Fig. 4 shows that the rather smooth and monotonic distributions seen in Figs. 2 and 3 are the results of superpositions of contributions from different impact parameters which have quite different shapes. Therefore, the dynamical approach as realized by QMD is essential in predicting such fragment distributions.

In Fig. 5 are shown the production cross sections of various fragments for the 1.5-GeV $p+{}^{56}$Fe reaction. The data were measured by Michel *et al.* [16] at 1.6 GeV for $^{\text{nat}}$Fe. It is clearly concluded that the QMD+SDM approach reproduces the fragment production cross sections in the whole mass region well, including the light clusters such as α and IMF ($A\sim$ 20–30) except for ^{7}Be where the present result underestimates the data by approximately 2 orders of magnitude.

A similar comparison was made for 2.6-GeV $p+{}^{56}$Fe reaction in Fig. 6. In this case, again, the overall agreement of the theoretical results with the data of Michel *et al.* [16] is encouraging. However, the production cross sections of ^{7}Be is underpredicted more than one order of magnitude as was the case at 1.5 GeV. Furthermore, the theory could not predict any production of ^{10}Be. Agreement at the IMF region is somewhat worse than the 1.5-GeV result, in particular shape of the production cross sections of Ne isotopes is not reproduced correctly. These problems, together with the problem of ^{7}Be production at 1.5 GeV, may by accounted for by the multifragmentation mechanism not included in the present model [16]. An explanation of the origin of the disagreement for ^{55}Co and ^{56}Co production cross sections will be given later.

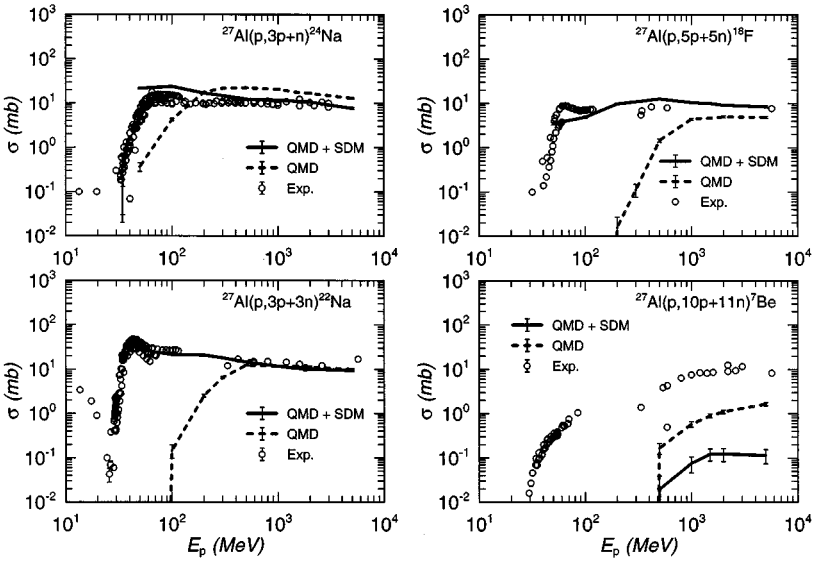

FIG. 8. Same as Fig. 5 but for the $p+^{27}$Al reaction.

The calculated isotope production cross sections from proton-induced reaction on ^{56}Fe and ^{27}Al are compared with experimental data in Figs. 7 and 8 for various residual nuclei as a function of incident energy in the energy region of 50 MeV to 5 GeV. We did not distinguish the experimental data for ^{56}Fe and ^{nat}Fe in order to enhance the experimental database. In these figures, the results of the QMD calculation is given by the broken curves, the QMD+SDM result by the solid curves, the experimental data by the open circles with error bars. The error bars in the QMD and QMD+SDM calculations indicate the statistical uncertainty. The experimental data have been retrieved from the CHESTOR (Charged Particle Experimental Data Storage and Retrieval System) database at Nuclear Data Center of JAERI [22] supplemented by available literatures including the recent data reported by Michel *et al.* [16].

The ^{56}Fe(p,x) cross sections shown in Fig. 7 again reveal the general accuracy of the QMD+SDM approach for the *a priori* estimation of production cross sections of targetlike fragment for a very wide incident energy range; the QMD+SDM calculation reproduces the experimental data within a factor of 2. In most cases, shapes of the prefragment production cross sections (the broken curves) are quite different from those of the final cross sections (solid curves) except for such a simple reaction as the (p,n) case where the prefragment production cross section is always larger than the final cross section by a constant ratio. The difference between the ''QMD'' and ''QMD+SDM'' calculations shows that the production of these fragments is a result of subtle balance between the dynamical formation and the statistical decay processes. The dynamical process acts as a ''source'' of ''hot'' prefragments at the target mass region, followed by the production of nuclides with smaller masses due to particle evaporation. It is intersting to note that the calculated ^{56}Fe$(p,n)^{56}$Co reaction cross section increases at energies above several hundred MeV. The same energy dependence was obtained for ^{56}Fe$(p,2n)^{55}$Co and ^{59}Co$(p,n)^{59}$Ni reactions. It is natural to assume that such reactions leading to the formation of prefragments which are very close to the target take place mostly at the peripheral region (as Fig. 4 clearly demonstrates). For these events the number of collisions in the compound system may be only 1 or 2. Then, the cross section for such events will be roughly proportional to the basic nucleon-nucleon cross sections adopted in the calculation. Indeed, the p-n cross section used in our calculation increases at the energy above 400 MeV due to contributions of the inelastic channels (see Fig. 1 of Ref. [1]). On the contrary, the recent data measured by Michel *et al.* [16] shows a steep drop above 1 GeV. However, the ^{nat}Fe$(p,xn)^{57}$Co and ^{nat}Fe$(p,xn)^{58}$Co reactions reported by them have a clear increase above several hundred MeV, although they attribute this energy dependence to the influence of secondary reactions. We hope that further experimental investigation of such reactions would be carried out to obtain information on this subject because it could be a direct measure of the NN inelastic collision in nuclei.

Figure 8 exhibits a result of the similar analysis for ^{27}Al target. The cross sections for production of targetlike fragments are reproduced very well by the QMD+SDM calculation. On the contrary, the production cross section of ^{7}Be is noticeably underestimated, even the threshold energy not being reproduced correctly. These results are consistent with the case for the $p+$Fe reaction as shown in Figs. 5 and 6. Other reaction mechanisms which are not taken into the present model, including the multifragmentation, might be the origin of production of such ''heavy'' clusters as ^{7}Be.

IV. SUMMARY

We have calculated the production cross sections of various residues for 1.5-GeV proton-induced reactions on ^{56}Fe in terms of the quantum moleculear dynamics (QMD) and the statistical decay model (SDM). It was found that the distribution of the fragments calculated by QMD alone and QMD+SDM differs considerably. The distribution after the QMD calculation alone has a broad maximum close to the target mass and a maximum at the very light mass region. This distribution is then smoothed out by the statistical decay along the stability line, filling the gap at the intermediate-mass-fragment (IMF) region.

The QMD calculation predicts the dynamical production of light fragments which is not possible with the ordinary

cascade model approach. Furthermore, it was found that the distribution of the fragments depends strongly on the impact parameter, showing the importance of the dynamical treatment as realized by QMD. It was also demonstrated that the present QMD+SDM results are quite robust against the change of the switching time from the QMD to SDM approach.

The calculated results for proton-induced fragment production cross sections on ^{56}Fe and ^{27}Al have been compared with experimental data in the energy range of 50 MeV to 5 GeV. A satisfactory overall agreement of the QMD+SDM calculation with the measured data is obtained, which confirmed the basic validity of the model and underlying parameters adopted in the present approach. The production cross sections of heavy clusters such as ^{7}Be, however, were underpredicted by about 2 orders of magnitude. These problems would show that other production mechanisms which are not included in this model may be needed to improve the agreement between the theory and experimental data. This problem, together with the high energy behavior of the ^{56}Fe$(p,n)^{56}$Co reaction, should be investigated further for a better understanding of the phenomena.

ACKNOWLEDGMENTS

Th authors wish to thank Dr. Hiroshi Takada and Dr. Peter P. Siegler of JAERI, and Dr. Shiori Furihata of Mitsubishi Research Institute for valuable discussions and comments.

[1] K. Niita, S. Chiba, T. Maruyama, T. Maruyama, H. Takada, T. Fukahori, Y. Nakahara, and A. Iwamoto, Phys. Rev. C **52**, 2620 (1995).
[2] M.B. Chadwick, S. Chiba, K. Niita, T. Maruyama, and A. Iwamoto, Phys. Rev. C **52**, 2800 (1995).
[3] S. Chiba, M.B. Chadwick, K. Niita, T. Maruyama, and A. Iwamoto, Phys. Rev. C **53**, 1824 (1996).
[4] J. Hüfner, Phys. Rep. **125**, 129 (1985).
[5] H.W. Barz, J.P. Bondorf, R. Donangelo, I.N. Mishustin, and H. Schulz, Nucl. Phys. **A448**, 753 (1986).
[6] A.S. Botvina, A.S. Iljinov, and I.N. Mishustin, Nucl. Phys. **A507**, 649 (1990).
[7] L.G. Moretto and G.J. Wozniak, Annu. Rev. Nucl. Part. Sci. **43**, 379 (1993).
[8] E. Gadioli and P.E. Hodgson, *Pre-Equilibrium Nuclear Reactions* (Clarendon Press, Oxford, 1992).
[9] K.H. Tanaka, Y. Yamanoi, H. Ochiishi, H. Akiyoshi, S. Kouda, H. Nakamura, S. Morinobu, Y. Tanaka, K. Kimura, T. Shibata, Y. Sugaya, K. Yasuda, H. Ito, and T. Murakami, Nucl. Phys. **A583**, 581 (1995).
[10] T. Nishida, Y. Nakahara, and T. Tsutsui, ''Development of a Nuclear Spallation Simulation Code and Calculations of Primary Spallation Products,'' Report JAERI-M 86-116, 1986.
[11] S. Pearlstein, Astrophys. J. **346**, 1049 (1989).
[12] L. Sihver, C.H. Tsao, R. Silbergerg, T. Kanai, and A.F. Barghouty, Phys. Rev. C **47**, 1225 (1993).
[13] H. Vonach, private communication.
[14] N. Shigyo, S. Sakaguchi, K. Ishibashi, and Y. Wakuta, J. Nucl. Sci. Technol. **32**, 1 (1995).
[15] R. Michel and P. Nagel, ''Specifications for an International Codes and Model Intercomparison for Intermediate Energy Activation Yields,'' Report NEA/NSC/DOC(95)8, OECD/NEA, 1995.
[16] R. Michel, M. Gloris, H.-J. Lange, I. Leya, M. Lüpke, U. Herpers, B. Dittrich-Hannen, R. Rösel, Th. Schiekel, D.Filges, P. Dragovitsch, M. Suter, H.-J.Hogmann, W. Wölfli, P.W. Kubik, H. Baur, and R. Wieler, Nucl. Instrum. Methods Phys. Res. B **103**, 183 (1995).
[17] M. Mizumoto and S. Tanaka, Report No. JAERI-Conf 95-017, 1995.
[18] T. Maruyama, A. Ohnishi, and H. Horiuchi, Phys. Rev. C **45**, 2355 (1992).
[19] R.J. Charity, M.A. McMahan, G.J. Wozniak, R.J. McDonald, L.G. Moretto, D.G. Sarantites, L.G. Sobotka, G. Guarino, A. Pantaleo, L. Fiore, A. Gobbi, and K.D. Hildenbrand, Nucl. Phys. **A483**, 371 (1988).
[20] H.W. Bertini, ''Monte Carlo Calculations on Intranuclear Cascades,'' Report ORNL-3383, 1963.
[21] Y. Nakahara and T. Tsutsui, ''A Simulation Code System for High Energy Nuclear Reactions and Nucleon-Meson Transport Processes,'' Report JAERI-M 82-198, 1982.
[22] T. Fukahori, ''CHESTOR,'' Charged Particle Experimental Data Storage and Retrieval system, unpublished.